

Term Project – Incompressible, Laminar Flow over a Rectangular Cavity

Logan Halstrom

PhD Graduate Student Researcher

Center for Human/Robot/Vehicle Integration and Performance

Department of Mechanical and Aerospace Engineering

University of California, Davis

Davis, California 95616

Email: ldhalstrom@ucdavis.edu

1 Problem Description

This analysis concerns the incompressible, laminar flow over a two-dimensional rectangular cavity, analogous to the case detailed by Mehta and Lavan and as seen in Fig 1. For this case, steady, Couette flow is imposed over the cavity at laminar Reynolds numbers creating vortical flow structures. The effect of cavity geometry is investigated by varying the aspect ratio (AR) of the cavity (defined as the height of the cavity divided by the length) as such $AR \in [0.5, 2, 5]$ for $Re = 100$. Additionally, the effect of Reynolds number is observed simulating the $AR = 0.5$ case for $Re \in [1, 100, 2000]$.

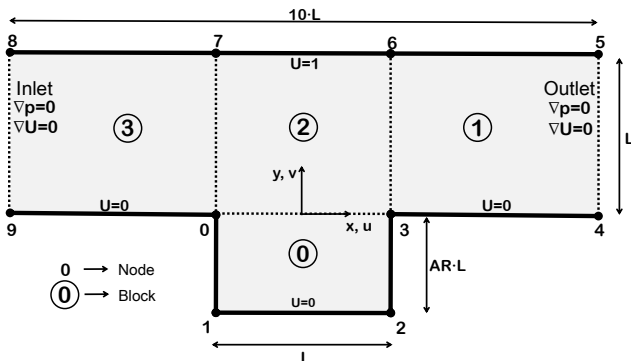


Fig. 1. Grid diagram for channel flow over cavity demonstrating dimensions, boundary conditions, and node and block indexing

2 Solution Approach

Solutions for all cases were obtained using the OpenFOAM flow solver version 2.3.0. Solver meshes were constructed according to the vertices and blocks described in Fig 1.

2.1 Solver Setup

For this study, the length of the cavity was chosen to be $L = 1$ and the length of the channel above the cavity was cho-

sen to be ten times that of the cavity so as to be representative of an infinite length. The upper channel (blocks 1 through 3) was designed to create the Couette flow upper boundary condition for the cavity, which is accomplished by setting a no-slip boundary condition at all walls and prescribing the upper wall with a positive x-direction velocity.

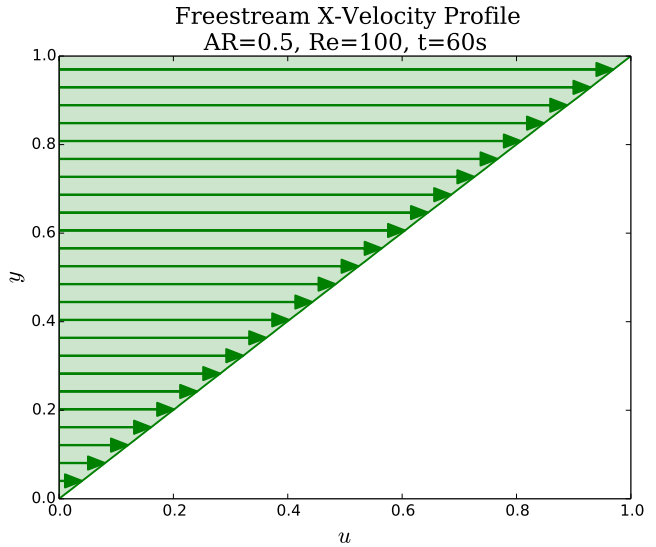


Fig. 2. Freestream velocity profile in channel upstream of cavity (Upper boundary condition of cavity)

The inlet and outlet are treated with zero gradient boundary conditions for pressure and velocity. Initial and boundary conditions can be found for each case in the $/0$ directory in the p and U dictionaries. This results in the linear velocity profile demonstrated in Fig 2, which is sampled at $x = -2.5$ for the $AR = 0.5$, $Re = 100$ case using the *sampleDict* dictionary created for this analysis and located in the */System* directory of each case. This dictionary samples u and v velocity profiles at the freestream and grid centerline locations

and is executed by calling first `foamCalc` components `U` to calculate the velocity field components of the solution and then calling `sampleDict` with `sample`. Channel flow was converged to this same profile for all cases.

OpenFOAM's transient, incompressible, laminar, Navier-Stokes solver `icoFoam` was selected for all cases in this analysis since all case Reynolds numbers were below 2300 and thus well within the laminar region. Some experimentation with the turbulent solver `pisoFoam` demonstrated that no turbulence effects appeared in the same cases by employing turbulent solver.

2.2 Mesh Grading

Meshes for each case were created using the *final-MakeDir.py* script which copies the base directory and rewrites the mesh and control dictionaries according to user inputs (including number of points in the cavity and channel blocks, grading of the channel, and start and end time of the run). Time step was selected according to the CFL condition for stability. The domain was divided into four separate blocks to allow for simple mesh grading within the channel. For each case, uniform and equal mesh spacing was used in x and y within the cavity (*Block 0*), while mesh size within the channel was continuously expanded in all directions away from the cavity. Thus for *Blocks 1* through *3*, y spacing at $y = 0$ was made equal to that of *Block 0* and then increased continuously along the height of the channel. x spacing of the cavity was matched in *Block 2* and at the edges of *Blocks 1* and *3* adjacent to *Block 2* and then expanded continuously away from the cavity.

Various mesh densities were investigated for optimal convergence, and little difference was observed in converged flow solutions for meshes finer than $dx = dy = 0.02$ in the cavity. Thus, this spacing was utilized for all cases, resulting in the meshes summarized in Table 2.2.

	dx	nx	ny	SR_y	N
<i>AR = 0.5</i>	0.02	50	25	1	$3.73e3$
<i>AR = 2</i>	0.02	50	100	1	$1.74e4$
<i>AR = 5</i>	0.02	50	250	1	$3.27e4$
Ultrafine-Uniform	0.001	1000	2000	1	$4.05e6$
Ultrafine-Graded	0.001	1000	300	25	$6.47e5$

Table 1. Mesh sizes for all cases (dx, nx, ny for *Block 0*, SR_y is y expansion ratio in cavity, and N is total number of points in grid. dx=dy in cavity for SR_y=1)

2.3 Solution Mapping

An ultra-fine mesh was required to resolve the bottom corner vortices in the cavity in the $AR = 2$ case. The increased fineness of the mesh within the cavity resulted

in a significant increase in the total number of grid points (4.05×10^6 points for a uniform cavity mesh). This number was reduced to 6.47×10^5 points (84% less) by adding grading to the cavity in the y -direction such that the y mesh spacing at the base of the cavity matched that of x and at the top of the cavity matched the original cavity spacing. Solutions on this mesh were derived by mapping the converged coarse mesh solution using the `mapFields` utility with `-consistent` mapping since the overall geometry was unchanged.

2.4 Parallel Computing

To increase the performance of the numeric solutions in this analysis, parallel processing was enabled using the *OpenMPI* implementation. For each case, the domain was decomposed into multiple subdomains according to the `decomposeParDict` dictionary using the `decomposePar` command. Domains must be decomposed into n_x and n_y sub-domains such that $n_x \times n_y$ is equal to the number of processors used in the computation.

Computations for this analysis were performed on an AMD Phenom II 1090T processor using all six cores available. During the simulations, it was noticed that solution speed would decrease with time, suggesting inadequate cooling. For future runs, it is recommended to use a lesser amount of cores for optimal performance with parallel computing. In OpenFOAM, parallel runs are executed with `mpirun -np <# of processors> icoFoam -parallel`, and after the solution is complete, the domain is recomposed with `reconstructPar`.

3 Results and Discussion

For each solution, streamlines were calculated from the converged velocity field and plotted using OpenFOAM's *Stream Tracer* function, and are presented in the following section. First the effect of Reynolds number was investigated for $AR = 0.5$. In all cases, a single, primary vortex forms within the cavity. For the $Re = 1$ case (Fig 6), the dividing streamline at the top of the cavity is concave or comes into the cavity, which is comparable with the results of Mehta and Zalman. Increasing the Reynolds number to $Re = 100$ (3), the dividing streamline is seen to become convex as the central vortex strength increases and the shear layer streamlines become more dense, which is also presented in the reference study. Finally, increasing to $Re = 2000$ (Fig 7), the central vortical region is observed to move to up and to the right, also described in the comparative study. This is due to the decreasing influence of viscous wall effects as the Reynolds number is increased.

Next, the effects of geometry on cavity flow were investigated by increasing the aspect ratio of the cavity for $Re = 100$. For these cases, the region of flow already observed in the $AR = 0.5$ case remain identical, but the new, lower portions of the geometry are filled with secondary vortical regions. In the $AR = 2$ case (Fig 4), a primary and secondary vortex form and are of comparable shape to those presented by Mehta and Zalman.

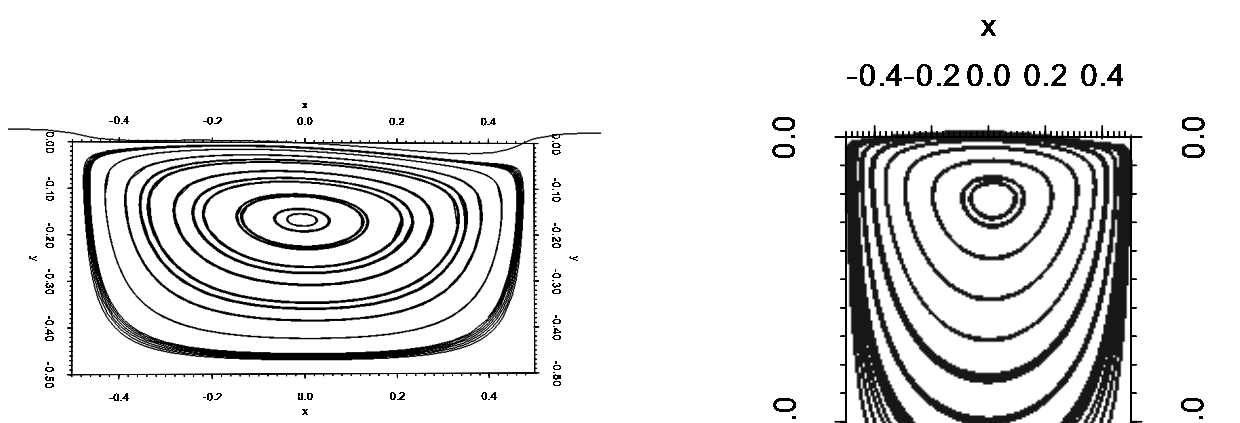


Fig. 3. Primary, central vortex for $AR = 0.5$, $Re = 100$ with convex dividing streamline

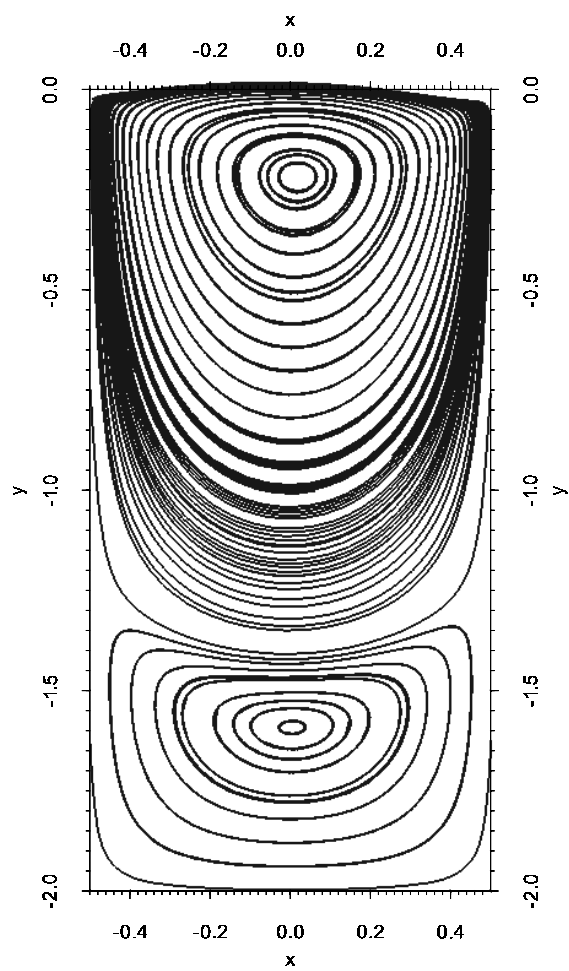


Fig. 4. Primary and secondary, central vortical regions for $AR = 2$, $Re = 100$ with convex dividing streamline

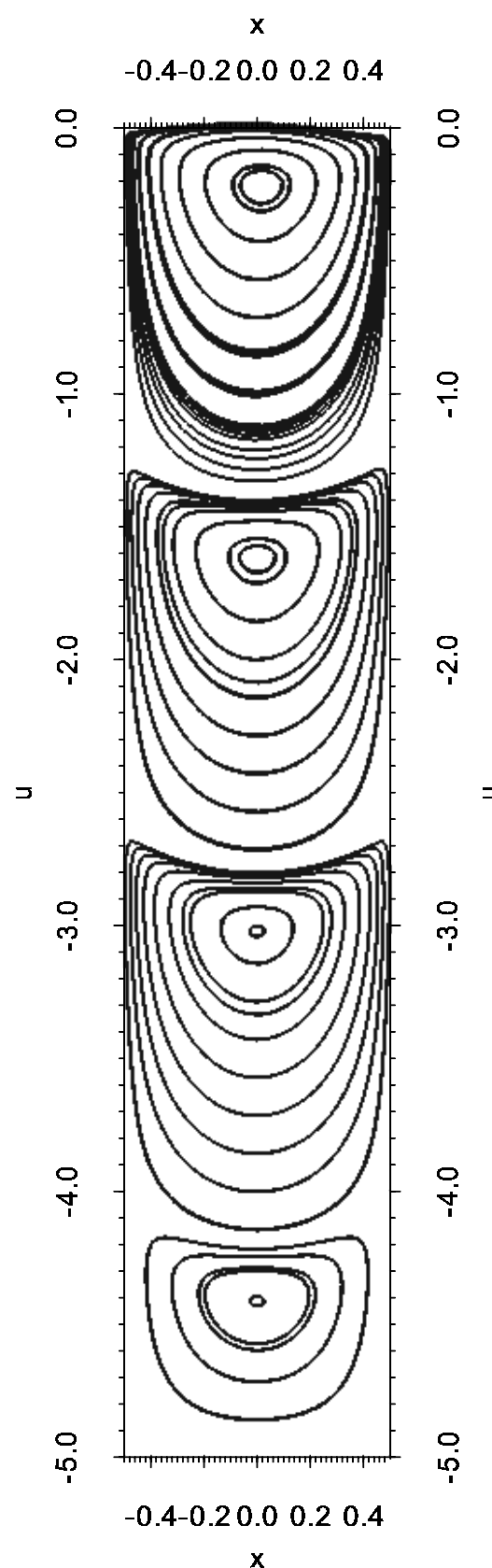


Fig. 5. Primary, secondary, tertiary, and quaternary vortical regions for $AR = 5$, $Re = 100$

The additional case of $AR = 5$ (Fig 5) was unique to this study and produced four vortical regions, with the first three of similar size and the last being much smaller than the rest and on the order of the size of the secondary vortex for the $AR = 2$ case.

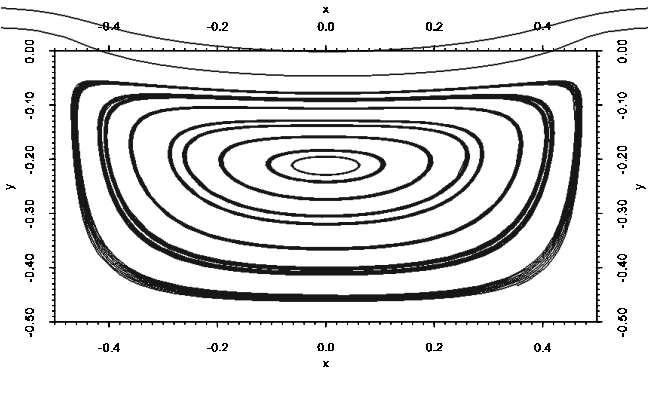


Fig. 6. Primary, central vortex for $AR = 0.5$, $Re = 1$ with concave dividing streamline

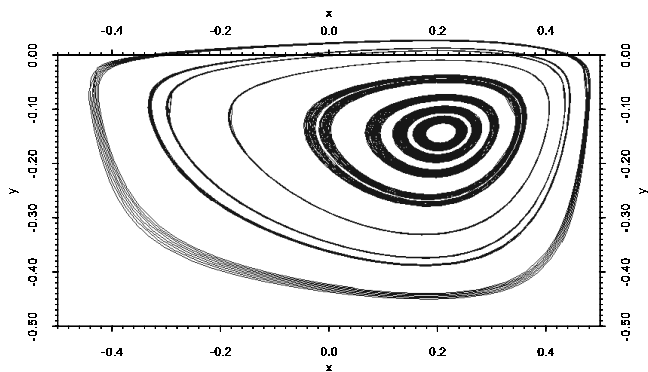


Fig. 7. Primary, offset vortex for $AR = 0.5$, $Re = 2000$ with convex dividing streamline

Finally, the structure of the bottom corner vortices for the $AR = 2$ case were investigated with a finer mesh for comparison with the results of Mehta and Zalman as shown in Fig 8. For the fine mesh in this study, right and left corner vortices were resolved that were of the same shape as the reference paper, but of approximately two-thirds the size. Larger corner vortices may be attainable using a finer mesh. Mehta and Zalman were additionally able to resolve secondary corner vortices after many subdivisions of their model. This should also be feasible using the method described in this paper, but using a much finer mesh. This analysis was omitted from this study and would be more feasibly accomplished by designing the mesh for x -direction mesh grading in the cavity and using a system with much more computational power.

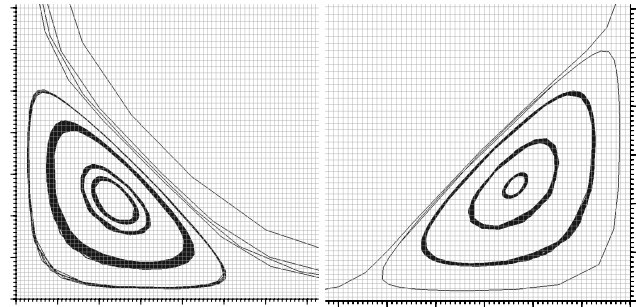


Fig. 8. Corner vortices for $AR = 2$, $Re = 100$ with grid superimposed (Large ticks are increments of 0.01)

4 Conclusion

This study details the setup and results of a Computational Fluid Dynamics (CFD) approach to the solution of incompressible, laminar flow over a two dimensional cavity. OpenFOAM solver results compared well to those of Mehta and Zalman in all cases. All solutions produced vortical regions within the cavity with additional secondary regions developing with increased cavity aspect ratio. For future implementations of this study, it would be beneficial to develop a more complex mesh system optimized for mesh grading to allow more efficient resolution of small vortical structures. Expansion into turbulent Reynolds numbers with a turbulent solver may also produce results of interest.

5 References

1. U. B. Mehta and Zalman Lavan. *Journal of Applied Mechanics*, 36(4):897-901, 12 1969.